ROYAL SOCIETY
OF CHEMISTRY

PAPER

Check for updates

Scalable one-step synthesis of gelatin–dithiolane for neural tissue engineering

Muhammad Waqas Ishaq,[a] Asma Talib Qureshi,[a] Saad Asim,[a] Akanksha Subbarao[a] and Muhammad Rizwan (ID) *[abc]

Protein-based hydrogels crosslinked using dithiolanes provide a promising viscoelastic matrix for soft tissue engineering and regenerative medicine including the neural niches due to their inherent biocompatibility, bioactivity, and adaptable extracellular matrix (ECM)-like viscoelastic behavior. Recently, we developed gelatin–dithiolane (GelDT) as a new class of ECM-mimicking viscoelastic hydrogels that displayed multi-functional properties, stimuli responsiveness and enabled independent tuning of the stiffness and matrix stress relaxation rate to precisely tune the matrix for improved cellular functions. However, the synthesis of GelDT remained laborious and inefficient. Herein, we report a scalable, one-step synthesis of GelDT that enables precise control over dithiolane functionalization (3–97%) using a carbonate–bicarbonate buffer system under mild aqueous conditions, while reducing organic solvent consumption from liters to the milliliters scale and eliminating the use of reducing agents. GelDT hydrogels obtained using the new synthesis route exhibit high stability (weeks), tunable stiffness, shear thinning, and self-healing properties essential for minimally invasive delivery. Additionally, pre-gelation tuning *via* physiochemical crosslinking allowed the fabrication of GelDT hydrogels at a remarkably low gelatin concentration (1.5% w/v) while ensuring fast gelation. The GelDT hydrogel supported the high viability and metabolic activity of encapsulated human iPSC-derived neural progenitor cell (NPC) spheroids. The GelDT hydrogel maintained NPC stemness (SOX2+, Ki-67+) and facilitated successful neuronal differentiation (MAP2+) in 3D culture. This work establishes a scalable, cytocompatible platform for producing dynamic protein-based hydrogels for regenerative medicine.

1. Introduction

The development of scaffolds that recapitulate the dynamic behavior and biochemical features of the native extracellular matrix (ECM) remains a key challenge in tissue engineering. This challenge is particularly noticeable in neural tissue engineering, where the matrix must simultaneously demonstrate low stiffness, viscoelasticity, injectability for minimally invasive delivery, and bioactivity to support neuronal survival and differentiation.[1–3] Traditional chemically crosslinked hydrogels are often mechanically strong, but they may lack the viscoelastic properties required to mimic the continuous remodeling of natural tissues. Conversely, physically crosslinked networks are shear-thinning and injectable; however, they lack matrix

stability required for 3D cell culture and are unable to provide mechanical stability *in vivo*.[2,4]

To address these limitations, dynamic covalent chemistry has emerged as a promising technique to crosslink the matrices that are stable, mechanically tunable, and yet provide an injectable matrix for minimally invasive therapeutic delivery.[5,6] Specifically, lipoic acid, a natural antioxidant, which contains a strained dithiolane ring, has garnered significant attention in recent years as a functional group to enable photoinitiator free, photo-crosslinking of hydrogels for tissue engineering applications.[7–9] Upon exposure to UV light, the dithiolane ring undergoes ring-opening polymerization to form linear disulfide bonds. Leveraging the unique properties of lipoic acid, our group recently developed a biomimetic gelatin–dithiolane (GelDT) hydrogel with ECM-like multifunctional properties[10] The dynamic disulfide bonds imparted self-healing properties, tunable viscoelasticity, and stress-relaxation properties to the GelDT hydrogel, offering a more cell-conducive tissue engineering scaffold compared to the static crosslinked gelatin hydrogel such as GelMA. Notably, the disulfide bonds respond to external stimuli such as thiols, UV light,[11] heat,[12] pH[13] and redox agents,[14] making them a promising platform for the development of stimuli responsive

[a] *Department of Biomedical Engineering, University of Texas Southwestern Medical Center, Dallas, Texas 75390, USA.*
  E-mail: muhammad.rizwan@UTSouthwestern.edu
[b] *Department of Ophthalmology, University of Texas Southwestern Medical Center, Dallas, TX, 75390, USA*
[c] *Harold C. Simmons Comprehensive Cancer Center, University of Texas Southwestern Medical Center, Dallas, TX, 75390, USA*

biomaterials. Unlike conventional thiol–ene or acrylate-based systems, lipoic acid-derived chemistry does not require photoinitiators or harsh reagents, enabling the cytocompatible fabrication of crosslinked networks under physiological conditions.[15,16]

Neural tissue engineering provides a compelling motivation for the development of dynamic, injectable, and bioactive gelatin-based dithiolane crosslinked matrices. Neural progenitor cells are highly sensitive to matrix stiffness, stress relaxation, and ligand presentation, which regulate neural cell functions and differentiation.[17] Covalently crosslinked hydrogels often impede neuronal spreading and maturation.[18,19] Dithiolane crosslinked hydrogels offer a unique opportunity to address these constraints by combining ECM-derived bioactivity with a stress-relaxing microenvironment at brain-relevant stiffness ranges.[20–22] Furthermore, the matrix stiffness and stress relaxation rate of the dithiolane crosslinked hydrogel can be precisely tuned independently to evaluate their effect on neural cells.[8,10,23]

Despite the promise of dithiolane-based hydrogels, current synthetic strategies to modify proteins such as gelatin with lipoic acid present significant challenges in scalability and translation. To date, protocols have relied on complex synthesis routes utilizing high volumes of organic solvents (such as DMSO) and reducing agents (such as β-mercaptoethanol) to prevent protein self-gelation during functionalization.[10] The use of β-mercaptoethanol is particularly problematic as it could disrupt the native disulfide bridges within the protein structure and lipoic acid, and poses toxicity concerns that require rigorous, time-consuming purification.[24] Furthermore, achieving precise control over the degree of functionalization (DoF)—a critical parameter for tuning hydrogel stiffness and degradation rates—remains difficult with existing methods. A simplified protocol for the synthesis of gelatin dithiolane hydrogels, with reproducible control over dithiolane grafting density, could improve the adoption of dithiolane-modified protein-based hydrogels for soft tissue engineering.

To address this challenge, in this study we introduce a robust, synthetic strategy for GelDT utilizing a carbonate–bicarbonate (CB) buffer system and N-hydroxysuccinimide (NHS) activated lipoic acid. This approach significantly reduces organic solvent consumption from liters to the mL scale and eliminates the need for β-mercaptoethanol. We demonstrate that this streamlined method offers precise control over the DoF (ranging from 3% to 97%) and enables the fabrication of hydrogels with highly tunable mechanical properties. Furthermore, we demonstrate that the synergistic combination of physical and photo-crosslinking stabilizes hydrogels at ultra-low precursor concentrations. These phenomena are potentially useful for neural tissue engineering, where highly porous, low-stiffness matrices are required to facilitate neurite outgrowth and nutrient diffusion. Guided by the mechanical and biological requirements of neural tissue engineering, we evaluated the performance of GelDT hydrogels as a 3D culture platform for human iPSC-derived neural cells. Furthermore, we examined the capacity of the hydrogel to maintain NPC stemness (SOX2 expression) and support neuronal differentiation (MAP2 expression) in a 3D environment. This work establishes a scalable, reproducible, and comparatively greener method for producing dynamic gelatin-based hydrogels, expanding their applicability in soft tissue engineering.

2. Experimental methods

2.1. Materials

Gelatin (type A, bloom strength: 120 g) (G1890), sodium carbonate (222321), sodium bicarbonate (S6014) and α-lipoic acid (LA) (T1395), MES (475893), N-hydroxy-succinimide (NHS) (130672), N-(3-dimethylaminopropyl)-N′-ethylcarbodiimide hydrochloride (EDC) (E7750), and Triton X-100 (T8787) were purchased from Sigma. α-Lipoic acid-NHS (LA-NHS) (A748349) was purchased from Ambeed. 4-Dimethylsulfoxide (D1284), bovine serum albumin (BP9703), and sodium hydroxide (1310-73-2) were purchased from Fisher Scientific. Resazurin solution (30025-2), Calcein-AM (80011-2) and Ethidium Homodimer I (40014) were purchased from Biotium. Dulbecco's phosphate-buffered saline (PBS) was purchased from Corning, NY, USA.

2.2. Synthesis of gelatin–dithiolane (GelDT)

2.2.1. Using lipoic acid (LA) (DMSO/MES solvent system). In a typical reaction, a $2\times$ molar excess of LA with respect to gelatin amines (185 mg of LA for 1.5 g of gelatin type A) was dissolved in a solvent mixture (8 mL DMSO:4 mL MES (0.1 M, pH 6)) at a ratio 2:1. Once dissolved, a $3\times$ molar excess of 1-ethyl-3-(3-dimethylaminopropyl) carbodiimide (EDC) (517 mg) and N-hydroxysuccinimide (NHS) (310 mg) with respect to LA moles was added to the dissolved LA solution. The reaction was left stirring for ≥ 25 h at room temperature (RT) while protected from light to activate LA while also eliminating any unreacted EDC. Next, 1.5 g of gelatin type A was dissolved in a solvent mixture (25.2 mL DMSO: 12.6 mL MES (0.1 M, pH 6)) at a ratio of 2:1 at 45–50 °C. Once dissolved, activated LA was added dropwise to the gelatin solution and the reaction mixture was left overnight (18–20 h) under stirring at 45–50 °C while being protected from light. The pH of the crude reaction mixture was adjusted to 9 using 1 M NaOH at the end of the reaction. Subsequently, the reaction mixture was dialyzed using the Spectra/Por 12–14 kDa MWCO dialysis tubing in MilliQ water, as described in Table S1, SI. The dialyzed solution was freeze dried and the conjugation of LA to gelatin was confirmed by proton nuclear magnetic resonance (^{1}H NMR) and attenuated total reflectance Fourier-transform infrared (ATR-FTIR) spectroscopy (Fig. S1) and the degree of functionalization (DoF (%)) was quantified using the 2,4,6-trinitrobenzene sulfonic acid (TNBS) assay following the vendor's instructions and calculated using a previously reported equation.[25]

$$DoF\ (\%) = \left(\frac{\text{absorbance of GelDT} - \text{absorbance of blank}}{\text{absorbance of gelatin} - \text{absorbance of blank}}\right) \times 100$$

2.2.2. Using the LA-NHS-ester (carbonate–bicarbonate (CB) buffer solvent system). CB buffer (0.25 M, pH 9) was made by dissolving 1911 mg of sodium carbonate (anhydrous) and 239 mg of sodium bicarbonate in 100 mL of MilliQ water.

The pH of the buffer was adjusted to 9 using 1 N HCL and 1 M NaOH. 1.5 g of Gelatin type A was dissolved in 38 mL of CB buffer at 50 °C. Once the gelatin solution was dissolved, 1.5 molar excess (205 mg) of α-Lipoic acid-NHS (LA-NHS) (for the highest DoF) was first dissolved at 20 mg mL^{-1} in 10 mL of DMSO and then added dropwise to the gelatin solution. The reaction was left stirring overnight (18–20 h), protected from light at 45–50 °C. Subsequently, the reaction mixture was dialyzed using the Spectra/Por 12–14 kDa MWCO dialysis tubing in MilliQ water, as described in Table S2, SI. Conjugation of LA and/or DoF (%) analysis was done as mentioned earlier.

2.3. Analytical characterization

The ^{1}H NMR spectra were recorded on a Bruker Advance Neo 400 MHz spectrometer. All spectra were recorded in deuterated water D$_2$O as the solvent and the ^{1}H NMR chemical shifts were reported as δ in units of parts per million (ppm). Fourier transform infrared (FTIR) spectroscopy was performed using a Nicolet™ Summit Pro spectrometer equipped with an Everest™ attenuated total reflectance (ATR) accessory. The spectra were collected in the mid-infrared region from 4000 to 400 cm^{-1} using 16 scans per spectrum.

2.4. Rheological characterization

Rheological characterization of GelDT was performed using a rheometer (MCR 302, Anton Paar, Austria). An Omnicure S2000 (Excelitas Technologies Corp., Waltham, MA, USA) containing a filter of wavelength λ = 365 nm and a 200-Watt mercury arc lamp ($\sim$30 W cm^{-2}) was used as the light source at an exposure distance of $\sim$2.5 cm. All measurements were taken thrice using 25 mm parallel-plate geometry, which was maintained at 37 °C with the help of the Peltier system. For time sweep measurements of photo-crosslinked GelDT, the precursor solution was loaded between the plates held at a 0.5 mm gap. The samples were conditioned at 37 °C for 2 min followed by 5 min of UV exposure to initiate dithiolane ring opening polymerization between the LA moieties. To demonstrate the physiochemical crosslinking in GelDT hydrogels, the GelDT precursor solution was loaded between 25 mm parallel plates (gap: 0.5 mm). The temperature was ramped down from 37 to 4 °C at 1 °C min^{-1} followed by incubation at 4 °C for 1 h to introduce physical gelation. Next, the physically gelled sample was exposed to UV light for 5 min to form disulfide crosslinks. A frequency sweep was performed to compare the storage (G') and loss modulus (G'') of GelDT hydrogels over a frequency range of 0.1–100 Hz at a strain of 1%. A flow sweep test was performed to evaluate the shear thinning behavior of GelDT hydrogels, where the shear rate was varied from 0.1 to 100 s^{-1}. To investigate the self-healing behavior of GelDT, a step-strain sweep test was performed where changes in G' and G'' under low (1%) and high (500%) strain were recorded for 60 s, respectively.

2.5. *In vitro* stability of GelDT gels

To test the stability of GelDT, gels prepared based on the DoF and in different concentrations of GelDT (10%, 7.5%, 5%, 2.5%, 2%, 1.75% and 1.5%) and GelDT+ (2%, 1.75% and 1.5%) were dissolved in PBS. Hydrogel samples (30 μL, n = 4) were prepared in 0.5 mL Eppendorf vials, which were weighed before (empty) and immediately after crosslinking; the mass was recorded as the initial gel mass (day 0). Next, the gels were incubated in PBS containing 0.5% sodium azide. The solution was removed each day, and the weight of the sample was recorded for 15 days. Prior to mass measurements, the samples were gently blotted with lint-free tissue to remove excess surface liquid without compressing the gels. The data were normalized to day 0 reading and were presented as the "normalized gel mass".

$$\text{Normalized gel mass} = \left(\frac{\text{gel mass}\,(d_x)}{\text{initial gel mass}(d_0)} \right)$$

On the other hand, to test gelation at ultra-low concentrations (0.5–2%), a vial inversion test was performed on photo-crosslinked GelDT and physiochemically crosslinked GelDT+.

2.6. 3D culture of PC12 cells

Rat PC-12 cells purchased from ATCC were cultured within a humidified incubator at 37 °C, in the recommended media. Upon reaching 80–90% confluency, the PC-12 cells were harvested and encapsulated in 2.5% and 5% GelDT with and without 3 mg mL^{-1} laminin–entactin (Corning) at a density of 1 × 10^6 cells per mL. Matrigel served as the control. The metabolic activity of encapsulated PC-12 cells was quantified using the resazurin assay (on days 1 and 7), according to the manufacturer's instructions. The GelDT biocompatibility was assessed through live/dead staining of encapsulated PC-12 cells on days 1 and 7 using Calcein-AM (live) and ethidium homodimer (dead) dyes, followed by visualization using an Olympus FV3000 confocal microscope.

2.7. 3D culture of human neuronal progenitor cells

Human iPSC-derived neuronal progenitor cells (iPSC-NPCs) (ATCC, ACS-5004) were cultured within a humidified incubator at 37 °C, in the recommended media. After reaching the desirable confluency, cells were dissociated using Stem-pro Accutase (Gibco) and seeded in an anti-adherent solution coated AggreWell plate to form iPSC-NPC spheroids ($\sim$800 cells per spheroid). These spheroids were collected and encapsulated in the GelDT hydrogel with and without 3 mg mL^{-1} laminin entactin (Corning) at a density of 100 spheroids per 100 μL and cultured for 7 days. On day 7, the biocompatibility of GelDT hydrogels with iPSC-NPC spheroids were monitored *via* a live/dead assay by staining with calcein-AM and ethidium homodimer-I. The spheroid morphology was observed by staining the F-Actin network with Phalloidin Alexa Fluor 647.

2.8. Neuronal differentiation of iPSC-NPC spheroids

To induce the neuronal differentiation in a 3D environment, iPSC-NPC spheroids were cultured in a neuronal induction medium comprising Neurobasal-A and DMEM/F12 (1:1)

supplemented with 1% N2 supplement, 2% B27 supplement, 1% GlutaMax, 20 ng mL^{-1} brain-derived neurotrophic factor (BDNF) (Acro Biosystems) and 20 ng mL^{-1} glial cell derived neurotrophic factor (GDNF) (Acro Biosystems) for 7 days. On day 7, the spheroids were fixed and stained with the MAP2 (mouse mAb, SC-74421, Santa Cruz Biotechnology) antibody, a neuronal marker, to evaluate the successful differentiation into neurons.

2.9. Immunocytochemistry

After a 7-day culture of NPC spheroids in GelDT hydrogels, the spheroids were fixed using 4% PFA for 45 minutes, followed by permeabilization using 0.5% Triton-X and were blocked using 3% BSA. The stemness and proliferative potential of the encapsulated NPC spheroids was monitored by immunostaining for SOX-2 (Rabbit mAb, 23064S, Cell signaling) and Ki-67 (MA5-14520, Invitrogen) antibodies, respectively. The samples were incubated overnight in primary antibodies (1:200), against Ki-67, SOX-2 and MAP2, at 4 °C, followed by incubation in anti-rabbit IgG Alexa Fluor 488 (Invitrogen, A11070) and anti-mouse IgG Alexa Fluor 488 (Invitrogen, A11017) secondary antibodies (1:1000) overnight at 4 °C. Nuclei were counterstained with DAPI. All samples were washed thrice with PBS for 30 minutes after each incubation step. The spheroids were imaged using an Olympus FV3000 confocal microscope. The expression was quantified by counting SOX2, Ki-67 and MAP2 positive cells and normalizing it to total nuclei to determine the percentage of positive cells, using ImageJ.

2.10. Statistical analysis

All statistical analyses were performed using GraphPad Prism version 8. Differences between the two dependent and independent groups were analyzed using paired and unpaired Student's t tests, respectively. Differences between more than two groups were analyzed either using one-way analysis of variance (ANOVA) or Tukey's *post hoc* test. A *P*-value of <0.05 was deemed statistically significant. No outliers were removed from the data analysis. The experiments were repeated using cells from different passage numbers and hydrogels from different batches. All the data are presented as mean $\pm$ S. D. Further information on the sample size, specific statistical tests for each experiment, and data presentation are provided in the figure captions. Three technical replicates were also included in each experiment.

3. Results and discussion

3.1. Synthesis of gelatin dithiolane using the carbonate–bicarbonate (CB) buffer system

Gelatin dithiolane (GelDT) hydrogel, formed by grafting lipoic acid (LA) onto gelatin chains followed by photo-crosslinking, provides a highly dynamic, photoinitiator-free hydrogel that supports 3D encapsulated cell culture and potential cell transplantation. GelDT combines inherent bio-adhesive and biodegradable properties with tunable mechanics that recapitulate the key features of physiological ECM remodeling. Our pioneering study previously reported he synthesis of GelDT and established the feasibility of GelDT hydrogels for tissue engineering.[10] However, it relied on the extensive use of organic solvents to improve solubility and β-mercaptoethanol to suppress undesired self-gelation of gelatin. In the present study, a streamlined synthetic strategy is introduced to minimize solvent use and remove the need for β-mercaptoethanol, while preserving the dynamic dithiolane functionality and overall hydrogel performance. We tested two different approaches to synthesize GelDT: (1) using LA and (2) using the LA-NHS-ester (LA with a terminal NHS ester group). In approach 1, carboxylic acid of LA was converted into an active succinimide ester using a previously reported DMSO/MES (2:1) solvent mixture.[10] The reaction was carried out at room temperature for at least 25 h to eliminate any unreacted EDC,[26] followed by mixing with gelatin to conjugate LA to gelatin *via* the amide bond (Fig. 1A). The reaction resulted in a high degree of functionalization (DoF; ~95%) with a ~78% yield (Fig. 1B) as confirmed by ^{1}H NMR where the peaks of methylene lysine protons (2H) ~2.9–3 ppm did not appear in the GelDT spectra (Fig. 1C). Furthermore, the FTIR spectra obtained for GelDT displayed characteristic amide bands: amide 1 (1633 cm^{-1}), amide 2 (1536 cm^{-1}) and amide 3 (1236 cm^{-1}), confirming the conjugation of gelatin lysine residues with LA (Fig. S1). This approach successfully eliminated the need for β-mercaptoethanol during GelDT synthesis; however, achieving a high DoF required at least a 2× molar excess of LA (to gelatin amines), and the excess LA precipitated during dialysis, unless the pH was adjusted during the dialysis process (Table S1).

In the second approach, we utilized lipoic acid with the NHS ester moiety and utilized carbonate–bicarbonate buffer (CB) as the solvent (pH ~9) to keep the gelatin lysine residues in a largely unprotonated state.[27,28] hypothesizing that the nucleophilic lysine residues will favor the amide bond formation with LA-NHS (Fig. 1D). Indeed, by simply mixing LA-NHS in gelatin solution (~pH 9) resulted in the formation of GelDT with precise control over the DoF (Fig. 1E). By varying the molar ratio of LA-NHS from a 0.3 to 1.5 molar excess with respect to gelatin amines, the DoF significantly increased from ~3% (amine:LA-NHS,1:0.3) to 97% (1:1.5) (Fig. 1E). This was further reflected in the FTIR spectra where characteristic amide group bands at 1632.89 cm^{-1}, 1530.72 cm^{-1} and 1239 cm^{-1} for amide I, amide II, and amide III showed an increased intensity with increasing DoF (Fig. 1F). The ^{1}H NMR spectra complemented these results, which showed a reduction in the intensity of methylene lysine protons with increasing DoF with complete disappearance observed at a high DoF of ~97% (Fig. 1G).

Together, these results show that both approaches generate GelDT without using β-mercaptoethanol, and the organic solvent use with the CB buffer system is drastically reduced (*e.g.* ~10 mL DMSO in this study compared to ~7.0 L in Asim *et al.*[10] for the entire synthesis), while preserving the reactive dithiolane group. Importantly, the LA-NHS route in CB buffer provided superior control over functionalization, higher reproducibility, and easier scalability. GelDT batches of up to at least
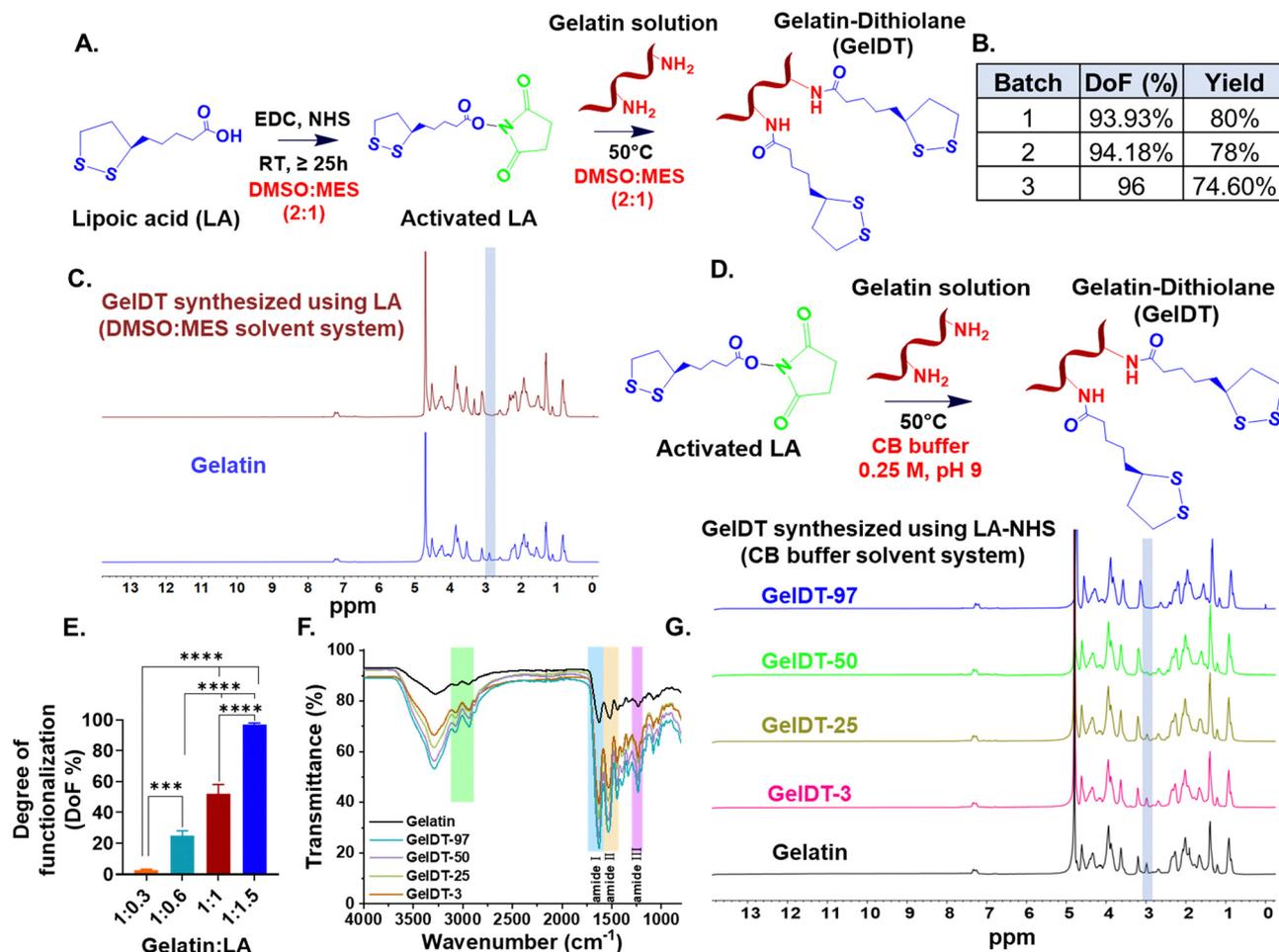
Fig. 1 (A) Schematic representation of GelDT synthesis using DMSO/MES as the solvent system with a (B) high yield and degree of functionalization (DoF (%)) without the need for β-mercaptoethanol. (C) ^{1}H NMR spectrum of GelDT in the D_2O, absence of the methylene lysine proton [2H] peak at ∼2.9 ppm represents a high degree of functionalization of lipoic acid. (D) Schematic representation of the facile synthesis of GelDT using activated LA (LA-NHS) and carbonate–bicarbonate (CB) buffer (0.25M, pH 9) as the solvent system. (E) Increasing the molar ratio of LA-NHS with respect to gelatin amine residues significantly increased the DoF (%) of GelDT, ***P =< 0.001, ****P < 0.0001, n = 3, mean ± S. D, one-way ANOVA, Tukey's post-hoc. (F) FTIR-spectra confirming the presence of characteristic amide bands at 1632.89 cm^{-1}, 1530.72 cm^{-1} and 1239 cm^{-1} for amide I, amide II, and amide III, respectively. (G) ^{1}H NMR spectrum of GelDT in D_2O. The peak intensity of the methylene lysine proton [2H] at 2.9–3 ppm decreased with increasing DoF confirming the increased conjugation of lipoic acid onto the gelatin chain with increasing LA-NHS moles relative to gelatin amine groups.

15 g were produced with a consistent DoF and yield without further optimization. β-mercaptoethanol is known to destabilize the protein structure by breaking the disulfide bonds leading to unfolding or partial denaturation. Because LA contains a five-membered dithiolane ring with a cyclic disulfide bond, the use of β-mercaptoethanol is undesirable as it can break this bond and compromise the UV (365 nm) reactive functionality of LA.[10] The streamlined LA-NHS/CB approach offers a more reliable method for preparing GelDT and can be potentially adapted to modify other proteins for dithiolane-based hydrogel formation. The GelDT was synthesized using the LA-NHS/CB buffer approach for the rest of the study.

3.2. Effect of the DoF (%) and precursor concentration on the gelation and stability of GelDT hydrogels

We first identified the minimum degree of functionalization (DoF) and prepolymer concentration required to form stable

GelDT hydrogels. Qualitative screening across a wide range of DoF (3–97%) and prepolymer concentrations (2.5–10% w/v) showed that GelDT with the lowest DoF (3%) at the lowest concentration (2.5%) failed to form a hydrogel, whereas all other formulations successfully gelled (Fig. 2A). Given the dynamic nature of disulfide crosslinks, hydrogel stability is a critical parameter for long-term cell culture and tissue regeneration applications. We therefore evaluated overnight stability in PBS at 37 °C for the same range of DoF and gelatin concentrations (Fig. 2B). Although GelDT-3 at 2.5–7.5% formed hydrogels initially (Fig. 2A), these formulations rapidly disintegrated during overnight incubation (Fig. 2B). In contrast, GelDT-3 at 10% gelatin content remained stable for at least 2 weeks, indicating that at the lowest DoF, 10% w/v represents the minimum concentration required for stable gel formation (Fig. S2). Increasing the DoF to 25–97% enabled hydrogel stability for at least 1 day across all tested gelatin concentrations (Fig. 2B).
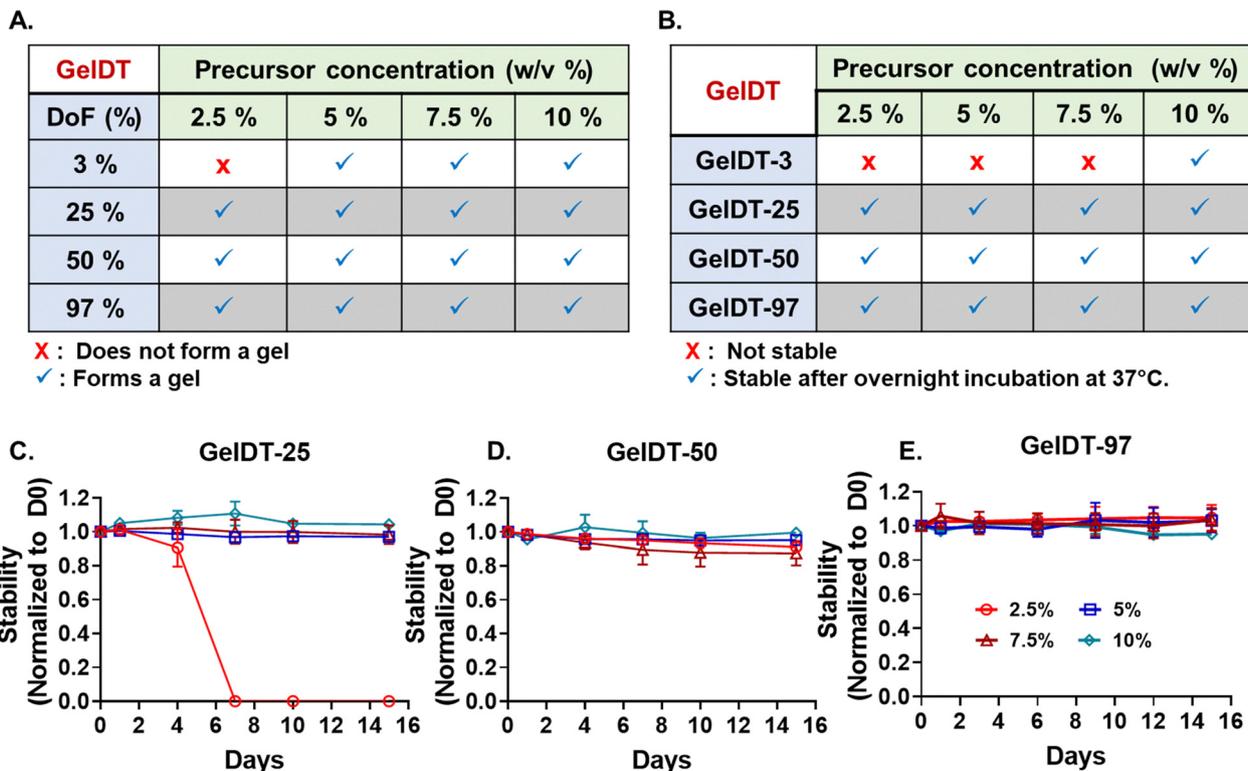
A.

GelDT	Precursor concentration (w/v %)			
DoF (%)	**2.5 %**	**5 %**	**7.5 %**	**10 %**
3 %	✗	✓	✓	✓
25 %	✓	✓	✓	✓
50 %	✓	✓	✓	✓
97 %	✓	✓	✓	✓

✗ : Does not form a gel
✓ : Forms a gel

B.

GelDT	Precursor concentration (w/v %)			
	2.5 %	**5 %**	**7.5 %**	**10 %**
GelDT-3	✗	✗	✗	✓
GelDT-25	✓	✓	✓	✓
GelDT-50	✓	✓	✓	✓
GelDT-97	✓	✓	✓	✓

✗ : Not stable
✓ : Stable after overnight incubation at 37°C.

Fig. 2 (A) Qualitative screening indicating that GelDT with a low DoF of 3% fails to form a hydrogel at a 2.5% polymer concentration, and a minimum concentration of 5% of GelDT-3 was required for gel formation. (B) Qualitative evaluation of the overnight stability of GelDT hydrogels with respect to varying DoF and prepolymer contents. Long-term stability of GelDT hydrogels under physiological conditions where (C) GelDT hydrogels (5–10% w/v) in the case of GelDT-25 and 2.5–10% in the case of (D) GelDT-50 and (E) GelDT-97 remained stable for atleast 2 weeks, n = 3, mean ± S. D.

However, extended stability studies revealed that GelDT-25 at 2.5% gelatin degraded within 2 days (Fig. 2C), while all other formulations remained intact for at least 2 weeks. At a 50–97% DoF, all GelDT formulations maintained structural integrity for at least 2 weeks regardless of the gelatin concentration (Fig. 2D and E).

Together, these results indicate that GelDT hydrogel stability is strongly governed by both the DoF and the gelatin content (wt%). Importantly, this tunability allows design of GelDT hydrogels to meet specific structural and temporal requirements for different tissue engineering applications. By adjusting the DoF and gelatin concentration, GelDT hydrogels can be fine-tuned to balance the initial gelation, long-term stability, and extent of dynamic disulfide crosslinks – key features for supporting cell growth and tissue regeneration.

3.3. GelDT displays the highly tunable gelation rate, biomechanical properties, and self-healing ability

We first investigated the photo-triggered gelation behavior of GelDT formulations (2.5, 5, and 10% w/v) using time-sweep rheology (Fig. 3A). Interestingly, 2.5% GelDT did not show any noticeable increase in the storage modulus G' when exposed to light (Light ON at 150 s mark). However, further increasing the prepolymer content to 5 and 10% resulted in rapidly initiated dithiolane ring-opening polymerization (approximately 10–30 s,) and converted into a transparent hydrogel but only at a DoF > 3%

(Fig. 3A and Fig. S3). Subsequent frequency-sweep measurements verified the development of a stable crosslinked network at 5 and 10% GelDT concentrations with a 25–97% DoF (Fig. S4). Next, we evaluated the effect of UV light intensity on gelation behavior, by irradiating a 10% w/v solution of GelDT-3 with the light intensity ranging from 4% to 100% using an Omincure S2000 light source. The *in situ* time-sweep rheology revealed a strong correlation between the UV light intensity and the onset of gelation, as determined by the increase of the G' (Fig. 3B). At the lowest tested intensity (4%), no gelation was observed, indicating that this light exposure was insufficient to trigger disulfide crosslinking. At an intermediate intensity of 25%, gelation occurred and the G' reached a plateau value of ≈11 Pa. Increasing the intensity to 50% yielded a plateau modulus of ≈110 Pa, eventually reaching 450 Pa at a 100% intensity (Fig. 3C). At lower UV intensities (25% and 50%), we posit that the reduced photon flux slows dithiolane ring opening (*i.e.* thiol radical generation), which reduces the attainable crosslink density within the given exposure period. In contrast, higher UV intensity increases dithiolane ring opening, which leads to more thiols available for disulfide crosslinking, resulting in a higher final G'. Therefore, the lower plateau modulus at reduced intensity is most likely due to an insufficient total UV dose and slower reaction kinetics rather than an intrinsic maximum modulus at that specific intensity. We anticipate that extending the irradiation time at lower intensity would further increase G' presumably due to increasing dithiolane ring opening.
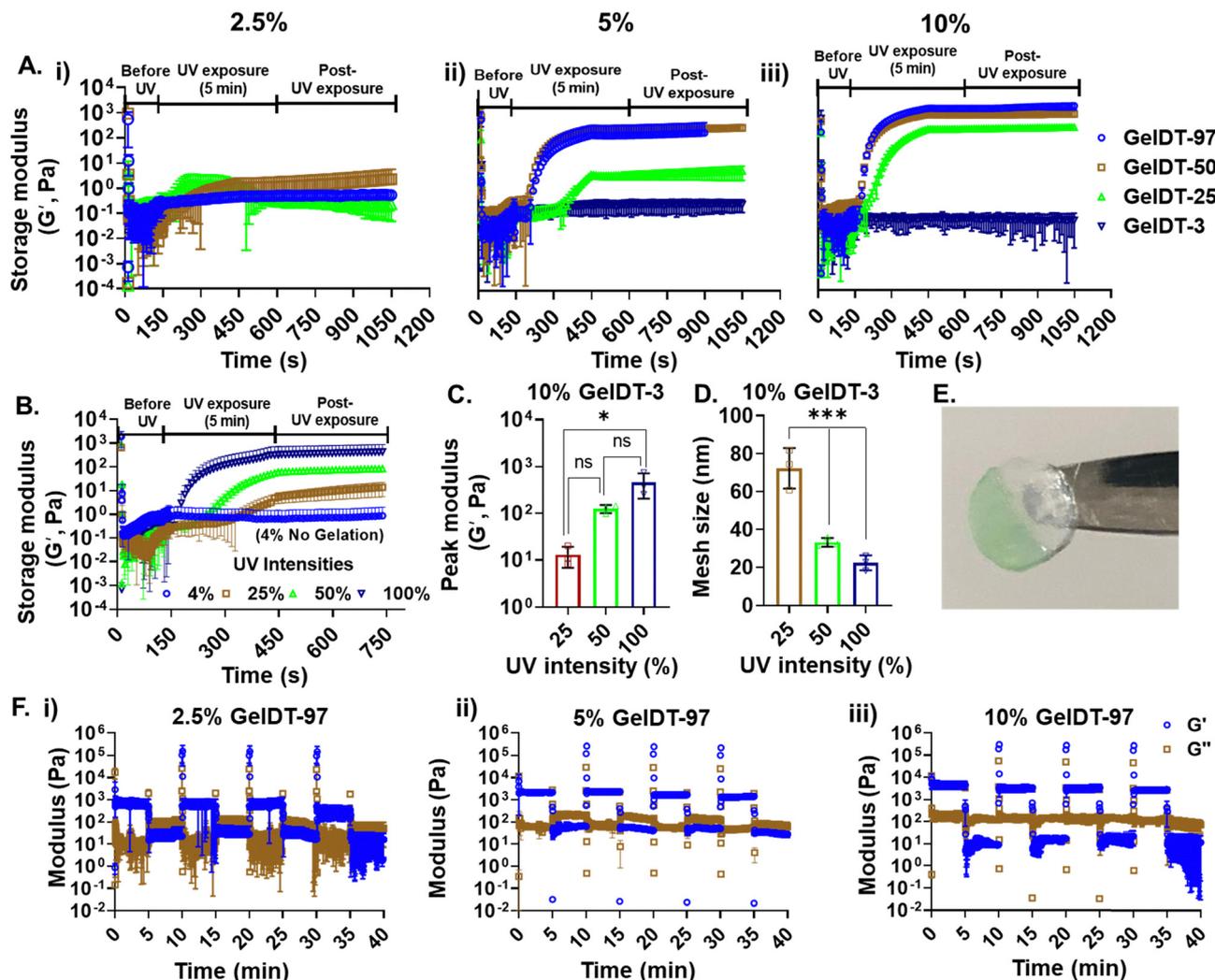
Fig. 3 (A) (i–iii) Time-sweep rheology of GelDT (2.5–10% w/v) precursors showing a real-time increase in the storage modulus (G') during photo-crosslinking upon UV exposure (5 min). G' increased due to disulfide crosslinks between LA moieties. (B) Effect of UV light exposure on the storage modulus (G') of a 10% w/v sample of GelDT-3. (C) Comparison of G' as the function of UV light exposure, *$P \leq 0.05$, $n = 3$, mean $\pm$ S. D, one-way ANOVA, Tukey's post-hoc. (D) Effect of UV light dose on the mesh size as estimated by the Peppas equation, ***$P \leq 0.001$, $n = 3$, mean $\pm$ S. D, one-way ANOVA, Tukey's post-hoc. (E) Qualitative assessment of the self-healing behavior of GelDT hydrogels *via* a cut and heal method, (F) Step-strain rheology of (i) 2.5%, (ii) 5%, and (iii) 10% GelDT-97 demonstrating the self-healing behavior when subjected to alternate cycles of low (1%) and high (500%) strains.

This interpretation is also supported by previous studies, which demonstrated that dithiolane ring opening, and thus crosslinking, can be modulated by using the UV exposure time.[8] Notably, this tunable range of hydrogel stiffness encompasses values relevant to 3D cell–matrix interaction studies, including mechanotransduction and differentiation in the context of soft tissues.[8,25,29] Furthermore, by using the Canal-Peppas equation,[30] an estimation of the mesh size revealed that the mesh size was inversely proportional to G' and the lowest mesh size of ~ 12 nm was observed for a maximum light intensity, as shown in (Fig. 3D).

A key requirement for injectable hydrogels is their ability to self-heal, enabling the network to rapidly re-establish crosslinks after the material experiences high shear forces during injection. This property is commonly achieved by incorporating dynamically reversible covalent linkages into the hydrogel structure.[31–33] Because GelDT hydrogels contain dynamic

disulfide bonds, we hypothesized that GelDT networks would exhibit intrinsic self-healing behavior. Qualitative assessment showed that when the GelDT hydrogel disc was cut into two pieces and freshly cut surfaces were brought into contact, they autonomously rejoined to form an intact construct (Fig. 3E). This was further supported by step-strain rheology where GelDT-97 hydrogels (2.5%, 5%, and 10% w/v) were subjected to alternate cycles of low shear strain (0.1%) and high shear strain (500%). Across all concentrations, the GelDT-97 hydrogels showed robust self-recovery, as indicated by the dramatic and repeatable transitions in G' and G'' between the high- and low-strain intervals (Fig. 3F(i-iii)). At 500% strain, G'' surpassed G', confirming that the crosslinks temporarily broke under deformation. When the strain was reduced back to 0.1%, G' rapidly exceeded G'' again, demonstrating the instantaneous reformation of the dithiolane-based reversible crosslinks.

The ability of the hydrogels to self-heal, *i.e.* reform crosslinked networks, is widely associated with the injectability of hydrogels.[32,33] Fig. S5 shows the ability of GelDT to serve as an injectable matrix for cell transplantation. Indeed, further experiments are required to demonstrate cell injection using GelDT hydrogels. Nonetheless, the results highlight the potential of GelDT as a matrix for applications involving minimally invasive therapeutic delivery to soft tissues such as the brain.

3.4. Physiochemical crosslinking enables the fabrication of GelDT hydrogels at an ultra-low gelatin content

We have previously reported the ability of the gelatin precursor to undergo physical gelation below room temperature with the photochemical crosslinking to significantly improve the strength of gelatin hydrogels and significantly reduce the gelatin content required to make a stable matrix.[10,25] However, the lowest gelatin content required to form a stable GelDT hydrogel matrix is still an open question. To answer this, we first systematically subjected 0.5–2% w/v GelDT precursors to dual physical–chemical crosslinking and evaluated gelation qualitatively using vial inversion tests (Fig. 4A). At prepolymer concentrations of 0.5%, control GelDT (photo-crosslinked) and

GelDT+ (dual crosslinked) did not form a gel. Further increasing the concentration to 1% formed a gel in the case of the GelDT+ hydrogel; however, the gel disintegrated after overnight incubation in PBS at 37 °C (Video S1). In contrast, physiochemical crosslinking enabled the formation of a stable hydrogel at a 1.5% pre-polymer concentration while photo-crosslinking alone induced partial to no gelation at this concentration. The 2% photo-crosslinked GelDT formed a hydrogel, but it failed to maintain the gelled state (Fig. 4A) (Video S2).

To understand how physiochemical crosslinking was modulating the gelation behavior, we performed rheology during *in situ* physiochemical crosslinking of GelDT precursor solutions (1.5–2%, Fig. 4B(i–iii)) and compared it against the photo-crosslinking only group (Fig. 4C(i–iii)). During the 4 °C incubation, surprisingly, the G' of the 1.5% precursor did not increase noticeably at the 4 °C phase, indicating that physical gelation does not occur, or is drastically slower, at ultra-low gelatin concentrations. Increasing the concentration to 1.75–2% resulted in the increase of G' that ultimately reached a plateau, indicating the completion of the sol–gel transition (physical gelation) (Fig. 4B(iii)). In contrast, direct UV exposure of the same precursor solutions resulted in no meaningful increase in
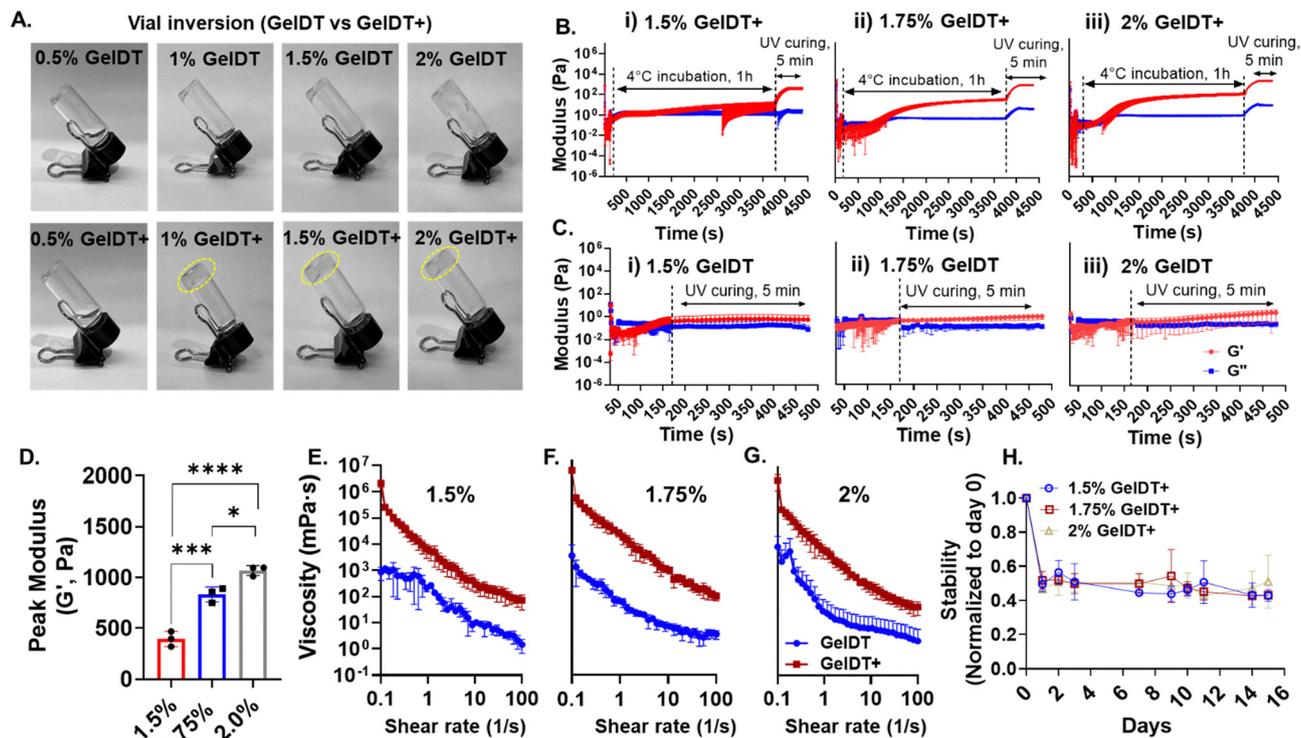

Fig. 4 (A) Vial inversion test indicating that the combination of physical gelation and photo-crosslinking allows the fabrication of stable hydrogels at an ultra-low gelatin content of 1.5%. (B) (i–iii) Time-sweep rheology (1.5–2%) of GelDT precursors showing a real-time increase in the storage modulus (G') during the 4 °C incubation followed by photo-crosslinking at 4 °C which further increased the G' due to disulfide crosslinks between LA moieties. (C) (i–iii) Time-sweep rheology (1.5–2%) of GelDT precursors subjected to photo-crosslinking only. (D) Quantitative comparison of G' of physiochemically crosslinked GelDT+ hydrogels at an ultra-low pre-polymer content with increasing the gelatin content from 1.5 to 2% resulting in increased G', **$P < 0.05$, ***$P = < 0.001$, and ****$P < 0.0001$, $n = 3$, mean ± S. D, one-way ANOVA, and Tukey's post-hoc. (E and G) Flow-sweep rheology indicating the shear-thinning behavior of ultra-low content GelDT+ hydrogels. (H) Comparison of the stability of photo-crosslinked GelDT and physiochemically crosslinked GelDT+ hydrogels over a period of 2 weeks, where GelDT+ hydrogels remained significantly stable compared to GelDT hydrogels, $n = 3$, and mean ± S. D.

G' for 1.5–2% GelDT, indicating the absence of the sol–gel transition (Fig. 4C). Furthermore, exposing the physically gelled matrices to photo-crosslinking resulted in the increase of G' due to dithiolane ring-opening polymerization, which was proportional to the gelatin concentration (Fig. 4D). This formation of hydrogels at an ultra-low gelatin content due to physiochemical crosslinking is attributed to the formation of partial-triple helical structures during physical gelation, which is likely to bring polymer chains into closer proximity and facilitate more efficient crosslinking between LA moieties upon UV exposure.[25,34] Importantly, this increase in network strength was further supported by stable G' observed across the tested frequency range (0.1–100 Hz) (Fig. S6). Consistent with this, GelDT+ hydrogels exhibited increased viscosity at a low shear rate and pronounced shear thinning behavior further confirming a cohesive yet injectable hydrogel network at ultra-low concentrations (Fig. 4E–G). Notably, this increased network strength of GelDT+ hydrogels also translated into the greater long-term stability of hydrogels, where 1.5–2% GelDT+ hydrogels remained stable for at least 2 weeks at physiological temperature (Fig. 4H). These results highlight that physical gelation and photo-crosslinking synergistically modulate the behavior of GelDT hydrogels, allowing ultra-low GelDT matrices to achieve mechanical integrity and stability that is not achievable through photo-crosslinking alone.

3.5. GelDT hydrogel supports the growth and viability of encapsulated neural progenitor cells

Injectable shear-thinning hydrogels represent a promising platform for neural cell transplantation because they enable the minimally invasive delivery of therapeutically relevant cells directly into damaged neural tissue. The dynamic nature of GelDT, stress-relaxation behavior, and tunable mechanical properties, provide a bioactive protein-based scaffold that can potentially protect encapsulated neural cells during transplantation and provide microenvironmental cues to maintain cellular viability and function *in situ*. To validate the suitability of GelDT for neural tissue engineering, we systematically evaluated its biocompatibility and ability to support the survival and stemness of encapsulated neural progenitor cells, critical parameters for successful cell therapy.[35–38] A soft microenvironment is known to better support the function of encapsulated neural cells.[37,39] Moreover, hydrogels must maintain stability under physiological conditions to enable long-term neural cell culture and differentiation. Based on these factors, we selected 2.5% and 5% GelDT hydrogels for neural cell studies, as they
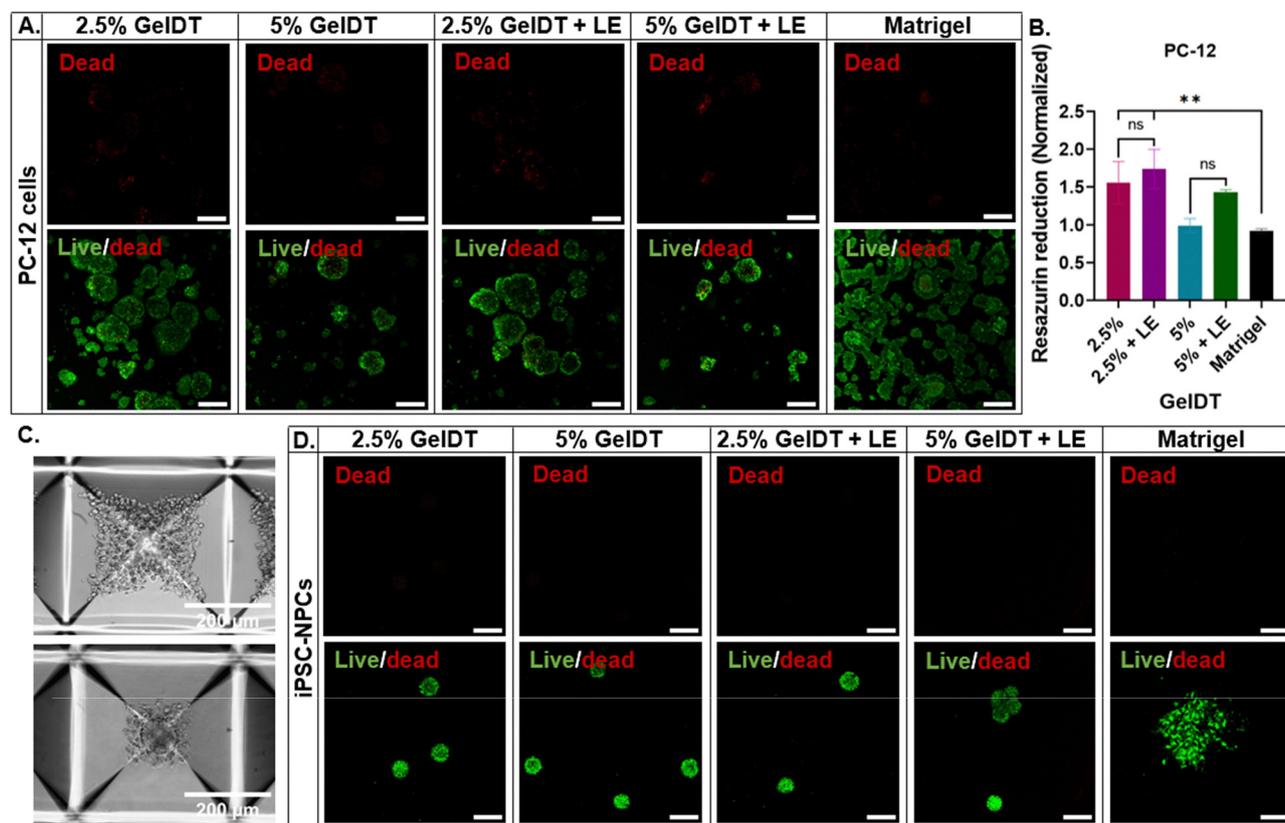

Fig. 5 GelDT hydrogels support the viability of encapsulated neuronal progenitor cells. (A) Live/dead assay performed on day 7 with PC-12 cells encapsulated in 2.5% GelDT, 5% GelDT, 2.5% GelDT + LE and 5% GelDT + LE hydrogels. (B) Metabolic activity of PC-12 cells encapsulated in 2.5% GelDT, 5% GelDT, 2.5% GelDT + LE and 5% GelDT + LE hydrogels, monitored on day 7 and normalized to day 1. $P** = <0.01$, $n = 3$, One-way ANOVA, and Tukey's post-hoc test. (C) Human iPSC-NPCs seeded in a 24-well AggreWell plate and centrifuged on day 1 to form compact spheroids by day 7. (D) Live/dead assay performed on day 7 with human iPSC-NPCs encapsulated in 2.5% GelDT, 5% GelDT, 2.5% GelDT + LE and 5% GelDT + LE hydrogels. LE = 3 mg mL^{-1} (Laminin entactin), scale bar = 200 μm.

demonstrated stability for at least two weeks (Fig. 2E) while maintaining a relatively low storage modulus (Fig. 3A). To test the biocompatibility of selected GelDT hydrogel groups, we first encapsulated PC-12 cells as a model neural progenitor cell and cultured them therein for 7 days. The live/dead assay indicated cell viability on day 1 indicating cytocompatibility for 3D cell encapsulation (Fig. S7). All GelDT hydrogel groups supported the survival of PC-12 cells in a 3D environment during the 7-day culture period (Fig. 5A). ECM proteins such as laminin are known to improve cell growth and functions.[40] Therefore, we compared the performance of GelDT with and without laminin entactin (LE) mixed in the 3D GelDT hydrogel matrix. Notably, GelDT without the LE group demonstrated similar growth and viability of PC-12 cells compared to GelDT-LE groups, likely due the fact that the GelDT matrix already provided a conducive protein-based environment (Fig. 5A). Furthermore, the metabolic activity of PC-12 cells demonstrated a statistically significant improvement in 2.5% GelDT groups compared to the Matrigel control. (Fig. 5B). Together, the data showed that GelDT hydrogels are biocompatible for 3D culture of PC-12 cells, particularly at lower polymer concentrations.

We next evaluated the culture of human iPSC-derived neural progenitor cells (iPSC-NPCs) for 7 days in 2.5% and 5% GelDT hydrogels with and without LE addition with Matrigel used as a control. The NPC spheroids of uniform size were formed using AggreWell plates (Fig. 5C). NPC spheroids maintained a high viability in all GelDT hydrogel groups without the formation of a necrotic core (Fig. 5D). The Inclusion of LE in the GelDT matrix did significantly change the viability or growth, which was in line with observations with PC12 cells. Intriguingly, the spheroid morphology was drastically different in the Matrigel group, where they did not maintain a compact shape, and started spreading in a 3D environment. This could be presumably due to the biochemical and biophysical cues offered by the Matrigel that regulate NPC behavior. Nonetheless, these results validate that GelDT is a conducive hydrogel matrix that supports the viability of human NPCs and can be potentially used for neural tissue engineering.[25,39,41–43]

3.6. GelDT maintains the stemness and proliferative potential of human iPSC-NPC spheroids

The maintenance of a robust proliferative activity along with the stemness in a 3D environment is essential for sustaining
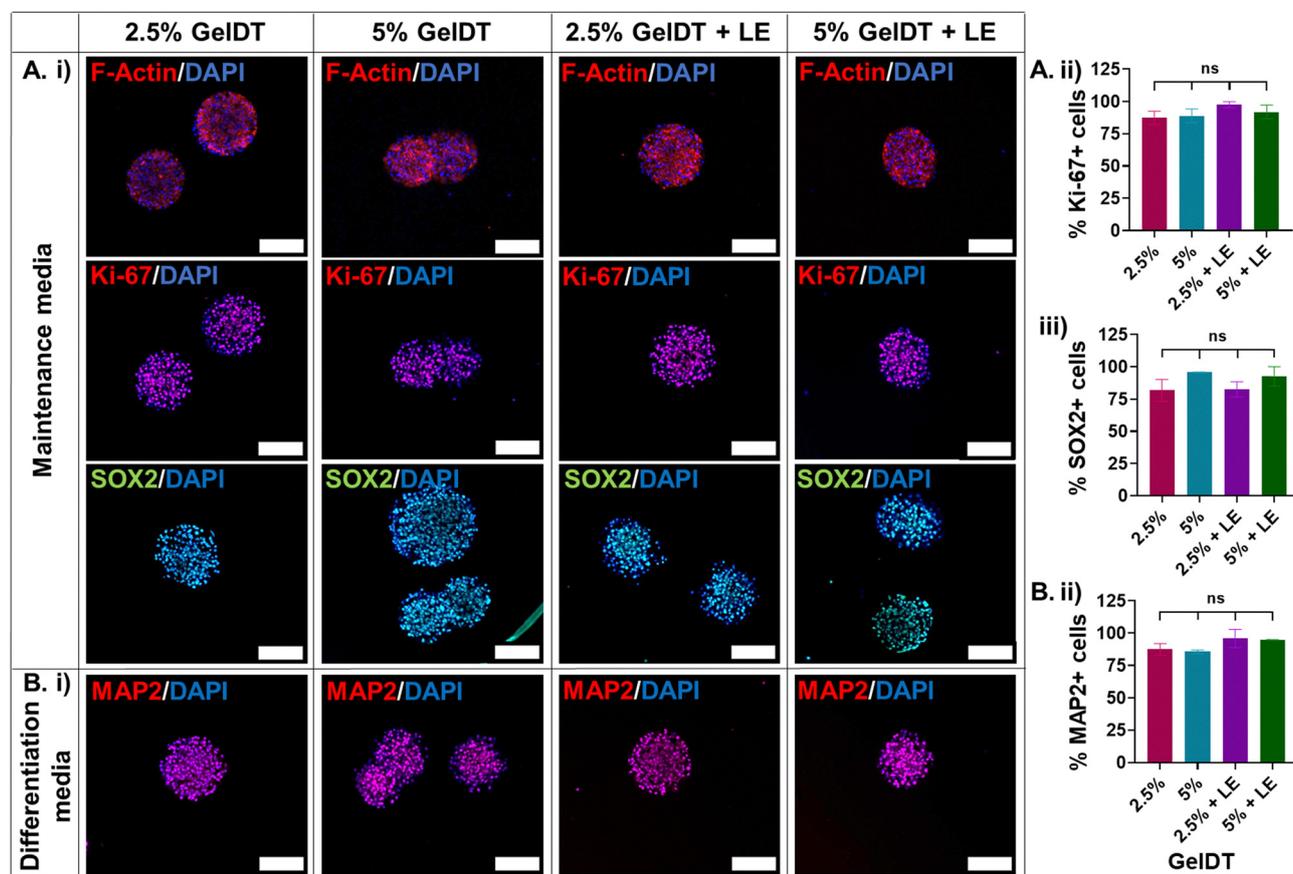

Fig. 6 GelDT hydrogel supports. (A) (i) The compact 3D spheroid architecture (F-Actin), proliferation (Ki-67), and stemness (SOX-2) of human iPSC-NPC spheroids encapsulated in 2.5% GelDT, 5% GelDT, 2.5% GelDT + LE and 5% GelDT + LE hydrogels (scale bar = 100 μm). (ii and iii) Quantification of Ki-67+ and SOX2+ cells from NPC spheroids cultured in 2.5% GelDT, 5% GelDT, 2.5% GelDT + LE and 5% GelDT + LE hydrogels. (B) (i) Neuronal differentiation (MAP2) of human iPSC-NPC spheroids (scale bar = 100 μm) and (ii) quantification of MAP2+ cells in NPC spheroids encapsulated in 2.5% GelDT, 5% GelDT, 2.5% GelDT + LE and 5% GelDT + LE hydrogels. $n = 3$, One-way ANOVA, and Tukey's multiple comparison tests.

the NPC's functionality *in vitro*.[43] To evaluate if the GelDT hydrogel could support these progenitor cell functions in a 3D environment, iPSC-NPC spheroids were cultured in 2.5% and 5% GelDT hydrogel groups for a week. After a 7-day culture period, the spheroids were fixed and stained with F-Actin to observe the 3D spheroid architecture, while Ki-67 and SOX-2 antibodies were used to evaluate their self-renewal potential and stemness, respectively. We observed that both the tested GelDT hydrogels exhibited a compact spheroid morphology and expressed Ki-67, supporting the proliferation of NPCs while SOX-2 expression showed the maintenance of their stemness in a 3D environment (Fig. 6A(i)). The quantification data revealed that more than 85% of the cells were in a proliferative state in both hydrogel compositions, while the 5% GelDT hydrogel group had a greater percentage ($\sim$95%) of SOX2+ cells than the 2.5% GelDT ($\sim$81%) group (Fig. 6A(ii and iii)). These results are in line with previous findings where NPCs encapsulated in dynamically crosslinked hydrogels retained the ability to self-renew and maintained the stemness of encapsulated NPCs due to matrix properties such as stress relaxation.[42,43]

To evaluate if the encapsulated NPC spheroids also retain the ability to differentiate into neurons, NPC spheroids were cultured in neuronal differentiation media for a period of 7 days, and then fixed and stained with the microtubule-associated protein 2 (MAP2) antibody. Both GelDT hydrogel formulations allowed the differentiation of encapsulated NPC spheroids, with more than 85% of MAP2+ cells indicating their differentiation ability (Fig. 6B(i and ii)).[44] Complementing the previous results, the inclusion of LE did not induce significant changes in the functions of iPSC-NPCs (Fig. 6).

While GelDT demonstrated excellent biocompatibility and the maintenance of neural stem cell functions in a 3D environment, further studies are required to investigate cell-matrix interactions and their effect on neuronal functionality. Furthermore, a comparison of a 3D supported matrix with 2D culture and matrix-free systems will help in identifying the critical role of matrix-mediated biophysical and biochemical cues on neuronal maturation and differentiation. Future studies will focus on the testing of GelDT as a biocompatible and injectable hydrogel platform for the delivery of NPCs in an *in vivo* neural injury model, as well as on the functional characterization of NPCs cultured in the GelDT matrix.

4. Conclusion

Gelatin dithiolane represents a protein based, ECM mimicking hydrogel system crosslinked through dynamic disulfide chemistry. In this work, we address the challenges in the synthesis of GelDT and demonstrate a significantly more efficient and simpler protocol to synthesize the GelDT matrix, while reducing the need for organic solvents and improving the scalability of GelDT fabrication. Our current GelDT synthesis method allowed precise control over the degree of functionalization (DoF) across a broad range (3–97%). By independently varying the DoF and gelatin content of the hydrogels, GelDT demonstrated tunability in the gelation behavior and stability of hydrogels with formulations of the DoF $\geq$25% demonstrating stability for at least 2 weeks at physiological temperature. Importantly, modulation of the DoF allowed us to tune the mechanical properties of GelDT hydrogels independent of the gelatin concentration. By further adjusting the UV light intensity, the mechanical properties of GelDT could be controlled independent of both the DoF and gelatin content. We also leveraged the physiochemical crosslinking capability of GelDT to fabricate ultra-low content (1.5% w/v), injectable GelDT hydrogels that exhibited remarkable stability for at 3 weeks. Finally, we highlighted the ability of GelDT to support the growth of PC12, human neural progenitor cells and spheroids with sustained viability for 7 days within the hydrogel matrix. Notably, immunostaining for MAP2 and SOX2 after 7 days revealed robust expression of both markers indicating preservation of the neural identity and maintenance of stemness in a 3D environment. Collectively, this work highlights GelDT as a versatile hydrogel platform that enables precise engineering of a dynamic 3D network for advanced tissue engineering applications.

Conflicts of interest

There are no conflicts to declare.

Data availability

Additional data are available from the corresponding author upon reasonable request.

The data supporting the findings of this study are available within the article and its supplementary information (SI). Supplementary information is available. See DOI: https://doi.org/10.1039/d5tb02915e.

Acknowledgements

References

1 O. Chaudhuri, L. Gu, D. Klumpers, M. Darnell, S. A. Bencherif, J. C. Weaver, N. Huebsch, H.-P. Lee, E. Lippens, G. N. Duda and D. J. Mooney, *Nat. Mater.*, 2016, **15**, 326–334.

2 J. Lou, R. Stowers, S. Nam, Y. Xia and O. Chaudhuri, *Biomaterials*, 2018, **154**, 213–222.

3 S. Nam, K. H. Hu, M. J. Butte and O. Chaudhuri, *Proc. Natl. Acad. Sci. U. S. A.*, 2016, **113**, 5492–5497.

4 Z. Wei, R. Schnellmann, H. C. Pruitt and S. Gerecht, *Cell Stem Cell*, 2020, **27**, 798–812.e796.

5 M. Rizwan, A. E. G. Baker and M. S. Shoichet, *Adv. Healthcare Mater.*, 2021, **10**, 2100234.

6 M. S. Huang, R. S. Navarro, L. G. Brunel, N. de Paiva Narciso, G. Aviles Rodriguez, N. J. Baugh, J. G. Roth, S. M. Hull, K. M. Hubka and S. C. Heilshorn, *Chem. Mater.*, 2025, **37**, 9758–9774.

7 B. R. Nelson, B. E. Kirkpatrick, N. P. Skillin, N. Di Caprio, J. S. Lee, L. P. Hibbard, G. K. Hach, A. Khang, T. J. White, J. A. Burdick, C. N. Bowman and K. S. Anseth, *Adv. Healthcare Mater.*, 2024, **13**, e2302925.

8 B. R. Nelson, B. E. Kirkpatrick, C. E. Miksch, M. D. Davidson, N. P. Skillin, G. K. Hach, A. Khang, S. N. Hummel, B. D. Fairbanks, J. A. Burdick, C. N. Bowman and K. S. Anseth, *Adv. Mater.*, 2024, **36**, 2211209.

9 G. A. Barcan, X. Zhang and R. M. Waymouth, *J. Am. Chem. Soc.*, 2015, **137**, 5650–5653.

10 S. Asim, C. Tuftee, A. T. Qureshi, R. Callaghan, M. L. Geary, M. Santra, V. Pal, I. Namli, G. H.-F. Yam, I. T. Ozbolat and M. Rizwan, *Adv. Funct. Mater.*, 2025, **35**, 2407522.

11 M. Ochmann, A. Hussain, I. von Ahnen, A. A. Cordones, K. Hong, J. H. Lee, R. Ma, K. Adamczyk, T. K. Kim, R. W. Schoenlein, O. Vendrell and N. Huse, *J. Am. Chem. Soc.*, 2018, **140**, 6554–6561.

12 H. Yu, Y. Wang, H. Yang, K. Peng and X. Zhang, *J. Mater. Chem. B*, 2017, **5**, 4121–4127.

13 G. Deng, F. Li, H. Yu, F. Liu, C. Liu, W. Sun, H. Jiang and Y. Chen, *ACS Macro Lett.*, 2012, **1**, 275–279.

14 H. F. Gilbert, *Methods in Enzymology*, Academic Press, 1995, vol. 251, pp. 8–28.

15 P. M. Kharkar, M. S. Rehmann, K. M. Skeens, E. Maverakis and A. M. Kloxin, *ACS Biomater. Sci. Eng.*, 2016, **2**, 165–179.

16 T. O. Machado, C. J. Stubbs, V. Chiaradia, M. A. Alraddadi, A. Brandolese, J. C. Worch and A. P. Dove, *Nature*, 2024, **629**, 1069–1074.

17 S. E. Stabenfeldt and M. C. LaPlaca, *Acta Biomater.*, 2011, **7**, 4102–4108.

18 E. M. Horn, M. Beaumont, X. Z. Shu, A. Harvey, G. D. Prestwich, K. M. Horn, A. R. Gibson, M. C. Preul and A. Panitch, *J. Neurosurg.*, 2007, **6**, 133–140.

19 S. R. Moxon, N. J. Corbett, K. Fisher, G. Potjewyd, M. Domingos and N. M. Hooper, *Mater. Sci. Eng. C*, 2019, **104**, 109904.

20 O. Chaudhuri, L. Gu, M. Darnell, D. Klumpers, S. A. Bencherif, J. C. Weaver, N. Huebsch and D. J. Mooney, *Nat. Commun.*, 2015, **6**, 6365.

21 N. D. Leipzig and M. S. Shoichet, *Biomaterials*, 2009, **30**, 6867–6878.

22 J. G. Roth, M. S. Huang, R. S. Navarro, J. T. Akram, B. L. LeSavage and S. C. Heilshorn, *Sci. Adv.*, 2023, **9**, eadh8313.

23 F. O. Afolabi, L. Y. He and C.-C. Lin, *Macromol. Biosci.*, 2026, **26**, e00400.

24 J.-Y. Chang, *J. Biol. Chem.*, 1997, **272**, 69–75.

25 S. Asim, E. Hayhurst, R. Callaghan and M. Rizwan, *Int. J. Biol. Macromol.*, 2024, **264**, 130657.

26 J. Van Hoorick, P. Gruber, M. Markovic, M. Rollot, G.-J. Graulus, M. Vagenende, M. Tromayer, J. Van Erps, H. Thienpont, J. C. Martins, S. Baudis, A. Ovsianikov, P. Dubruel and S. Van Vlierberghe, *Macromol. Rapid Commun.*, 2018, **39**, 1800181.

27 H. Shirahama, B. H. Lee, L. P. Tan and N.-J. Cho, *Sci. Rep.*, 2016, **6**, 31036.

28 B. H. Lee, H. Shirahama, N.-J. Cho and L. P. Tan, *RSC Adv.*, 2015, **5**, 106094–106097.

29 S. Zhang, Y. Pan, Z. Mao, J. Zhang, K. Zhang, J. Yin and C. Wang, *Bioeng. Transl. Med.*, 2023, **8**, e10402.

30 T. Canal and N. A. Peppas, *J. Biomed. Mater. Res.*, 1989, **23**, 1183–1193.

31 P. Bertsch, M. Diba, D. J. Mooney and S. C. G. Leeuwenburgh, *Chem. Rev.*, 2023, **123**, 834–873.

32 S. Afrin, O. Siddiqua Prova, A. T. Qureshi, M. W. Ishaq, C. E. Callmann and M. Rizwan, *Biomaterials*, 2026, **326**, 123649.

33 A. T. Qureshi, S. Afrin, S. Asim and M. Rizwan, *Adv. Healthcare Mater.*, 2025, **14**, 2405260.

34 M. Rizwan, G. S. L. Peh, H.-P. Ang, N. C. Lwin, K. Adnan, J. S. Mehta, W. S. Tan and E. K. F. Yim, *Biomaterials*, 2017, **120**, 139–154.

35 D. R. Nisbet, K. E. Crompton, M. K. Horne, D. I. Finkelstein and J. S. Forsythe, *J. Biomed. Mater. Res., Part B*, 2008, **87**, 251–263.

36 S. Goldman, *Nat. Biotechnol.*, 2005, **23**, 862–871.

37 C. M. Madl, B. L. LeSavage, R. E. Dewi, C. B. Dinh, R. S. Stowers, M. Khariton, K. J. Lampe, D. Nguyen, O. Chaudhuri, A. Enejder and S. C. Heilshorn, *Nat. Mater.*, 2017, **16**, 1233–1242.

38 C. M. Madl, B. L. LeSavage, R. E. Dewi, K. J. Lampe and S. C. Heilshorn, *Adv. Sci.*, 2019, **6**, 1801716.

39 A. Banerjee, M. Arha, S. Choudhary, R. S. Ashton, S. R. Bhatia, D. V. Schaffer and R. S. Kane, *Biomaterials*, 2009, **30**, 4695–4699.

40 M. Rizwan, C. Ling, C. Guo, T. Liu, J. X. Jiang, C. E. Bear, S. Ogawa and M. S. Shoichet, *Adv. Healthcare Mater.*, 2022, **11**, 2200880.

41 K. Saha, A. J. Keung, E. F. Irwin, Y. Li, L. Little, D. V. Schaffer and K. E. Healy, *Biophys. J.*, 2008, **95**, 4426–4438.

42 M. S. Huang, B. L. LeSavage, S. Ghorbani, A. E. Gilchrist, J. G. Roth, C. Huerta-López, E. A. Mozipo, R. S. Navarro and S. C. Heilshorn, *Nat. Commun.*, 2025, **16**, 5213.

43 J. G. Roth, M. S. Huang, R. S. Navarro, J. T. Akram, B. L. LeSavage and S. C. Heilshorn, *Sci. Adv.*, 2023, **9**, eadh8313.

44 C. M. Madl, B. L. LeSavage, R. E. Dewi, C. B. Dinh, R. S. Stowers, M. Khariton, K. J. Lampe, D. Nguyen, O. Chaudhuri and A. Enejder, *Nat. Mater.*, 2017, **16**, 1233–1242.